JOURNAL OF MATERIALS SCIENCE 19 (1984) 1296–1306

A surface dislocation model of wear

M. J. MARCINKOWSKI
Department of Mechanical Engineering and Engineering Materials Group, University of Maryland, College Park, Maryland 20742, USA

A model of sliding wear, based upon the concept of surface dislocations, has been proposed. In particular, a dislocation cell structure is created in the plastically deformed surface layer, which in turn gives rise to shear crack initiation at the interface between this surface layer and the undeformed interior of the body. These shear cracks then grow with subsequent delamination of the surface layers. It is shown that the most important parameter in this theory is the rate of work hardening of the materials in question.

1. Introduction

The problem of wear is essentially one of surface deformation and involves both elastic and plastic distortions. A unified theory of deformation has been developed within the last few years wherein any distortion can be described in terms of some suitable and unique distribution of surface dislocations [1, 2]. It should thus be possible in principle to develop a surface dislocation model of wear which is both physically exact and mathematically precise.

Within recent years, various dislocation models have been proposed to account for sliding or adhesive wear [3–8]. They are all based upon the formation of a shear crack at some distance below the wear surface, whose growth leads to subsequent delamination of the plastically deformed surface layer. Crack formation has in turn been related to the formation of cell walls [9–12]. The mechanism of cell wall formation is however at present somewhat obscure, from which it follows that crack formation therefrom is even more difficult to account for. A detailed theory of wear via the delamination mechanism will be presented in the following sections which overcomes these various conceptual obstacles.

2. Basic distortions

Since the wear process consists of two surfaces that are in contact and moving relative to one another, such as the standard pin-on-disc, it seems reasonable to assume that the principal distortions will be those of simple compression or shear, or combinations thereof. We shall therefore consider such distortions in some detail. Fig. 1a, for example, shows an undeformed reference body which subsequently undergoes a simple elastic compression in response to the stress σ so as to generate the configuration shown in Fig. 1b. It has been shown [1, 2, 13] that the state of elastic stress represented in Fig. 1b can be described in terms of two sets of surface dislocations which are dotted in the figure. The inner or primary array of dislocations accounts for the primary distortion within the body, i.e. its vertical contraction, whereas the outer or secondary surface dislocation array relates to the barrelling effect associated with the body, i.e. the lateral expansion. Both surface dislocation arrays are in fact comprised of continuous distributions of dislocations of infinitesimal Burgers vectors.

In order to relieve the high internal stresses occasioned by the surface dislocations, crystal lattice dislocations with discrete Burgers vectors are generated within the interior of the body such as shown by the solid symbols in Fig. 1c. These lattice dislocations climb to the surface of the body and combine with both the primary and secondary surface dislocations to either eleminate or add respectively a length L of surface element, i.e. a plane of atoms, in accordance with the following reaction:

$$b_L + \sum b_s \leftrightharpoons L \tag{1}$$

where b_L is the Burgers vector of the lattice

0022–2461/84 $03.00 + .12

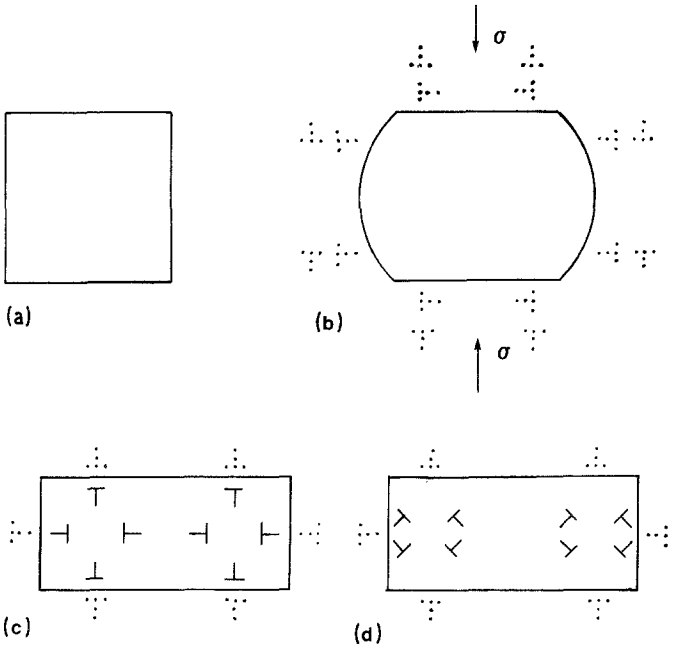

Figure 1 Reference block (a) in the undeformed state, (b) subjected to simple elastic compression, and (c) after plastic compression and with stress removed. (d) Same as (c), but with slip on planes at 45° to the compression axis.

dislocation, while b_s is that associated with the surface dislocations. It also follows that $b_L = -\Sigma b_s$ while $|b_L| = L$. Equation 1 is thus the basis of plastic deformation, and although it has been described with respect to the pure dislocation climb mechanism of Fig. 1c, the equivalent distortion could also have been produced by pure dislocation glide as portrayed in Fig. 1d. In this latter case, the dislocations are shown to move on places of maximum resolved shear stress, i.e. planes inclined at 45° with the horizontal. Even after the applied load is removed, such as in Figs. 1c and d, some of the surface dislocations still remain so as to satisfy the stress-free boundary conditions arising from those lattice dislocations which still remain within the body, i.e. have not yet reached the surface and undergone the reactions in accordance with Equation 1.

The second important mode of deformation with which we shall be concerned is illustrated in Fig. 2 where the undeformed reference block Fig. 2a is subjected to a simple elastic shear stress

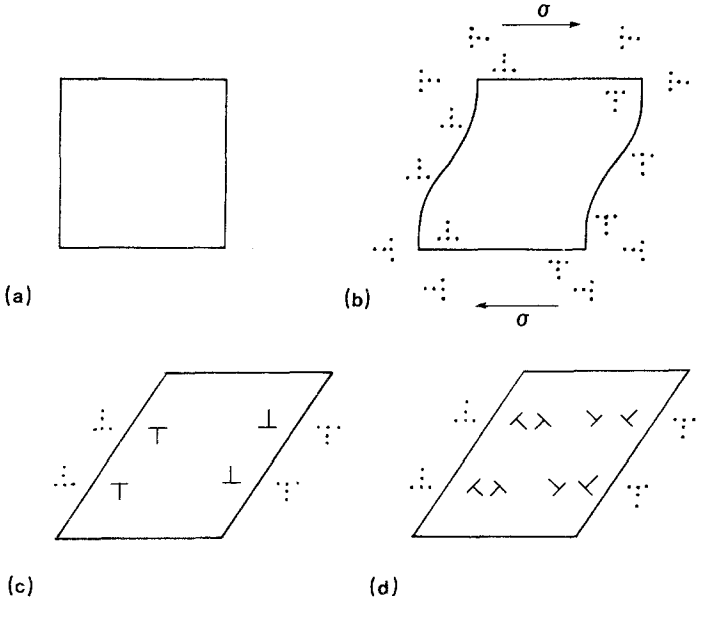

Figure 2 Block (a) in the undeformed state, (b) elastically deformed in response to a simple shear stress, and (c) plastically deformed with stress removed. (d) Same as (c), but with slip on planes at 45° to the shear direction.

σ to generate the configuration shown in Fig. 2b. The inner set of surface dislocations, which are again shown dotted, correspond to the primary array and account for the primary distortion which manifests itself in the rotation of the vertical faces of the body [1, 2, 13]. The outer, or secondary surface dislocation array, in Fig. 2b is related to the distortions on the horizontal faces of the body, upon which the stress σ is applied, and corresponds to a slight rotation of these faces. It is thus sufficient in this case to show only the effects of the single set of primary dislocations. In particular, as in the case already described with respect to Fig. 1, these surface dislocations can induce the generation of lattice dislocations within the body which in turn glide to the surface and give rise to the reaction expressed by Equation 1 to produce the plastically deformed state shown in Fig. 2c, i.e. a state of pure simple plastic shear. In this case, the length L in Equation 1 corresponds to steps or ledges on the vertical faces of the deformed body. The plastic distortion of Fig. 2c can also be produced by the generation of lattice dislocations on planes oriented 45° with respect to the shear direction as indicated in Fig. 2d. In this respect, Fig. 2d corresponds to Fig. 1d.

3. Cell wall formation

At sufficiently high plastic strains, the dislocations within the crystal arrange themselves into well-defined walls, in turn giving rise to the formation of virtually dislocation-free cells [14–18]. The observation that there is considerable misorientation across some of the cell walls has led to the formation of a model of cell wall formation based upon the theory of grain boundaries [19]. On the other hand, the density of dislocations at the cell walls, especially at high strains [14, 16], is so enormous that their description solely in terms of grain boundaries seems inappropriate. In order to overcome this difficulty, let us consider the formation of the cell wall configuration depicted in Fig. 3a, in response to the compressive stress σ. Here, it is assumed that slip occurs on a single system within each cell, and on one of two planes at 45° to the applied stress, i.e. the plane of maximum resolved shear stress. Such will be the case if the crystal is not oriented exactly as shown in Fig. 3a, and/or if local stresses give rise to a bias towards one of the two slip systems. The dislocations which comprise the cell wall in this figure are the resultant of the combination of dislocations from the two adjacent cells, and they are clearly seen to generate tilt-type boundaries.

If, on the other hand, slip occurs simultaneously within each individual cell on the two available slip systems, the cell wall configuration depicted in Fig. 3b will obtain. In this case, the cell walls consist of arrays of dislocation dipoles, with no misorientation across the walls. At the later stages of cell wall formation, it would seem that the

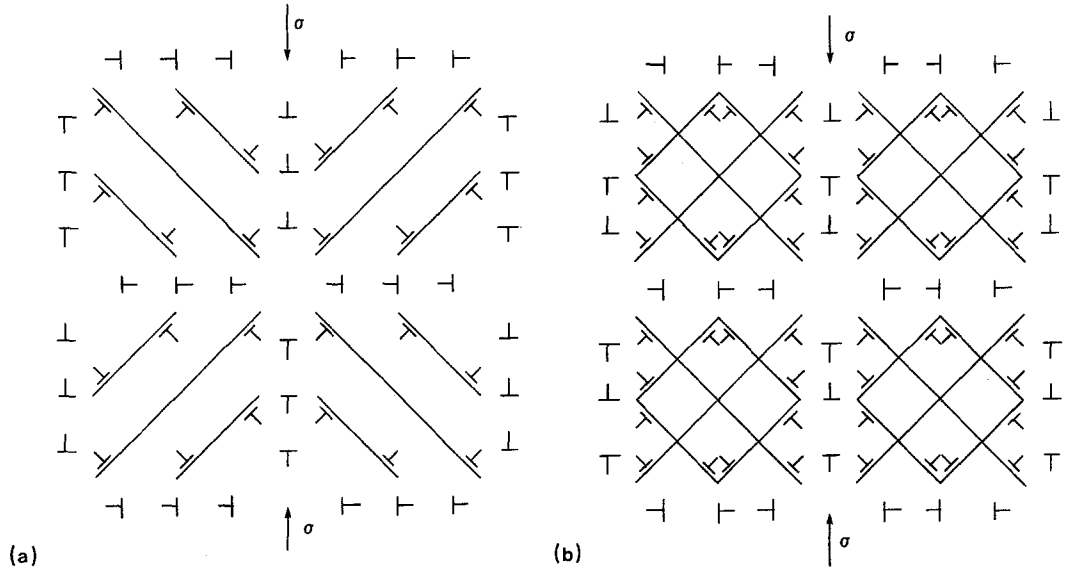

Figure 3 Cell wall formation in two dimensions under compression via (a) tilt boundary and (b) dipole formation.

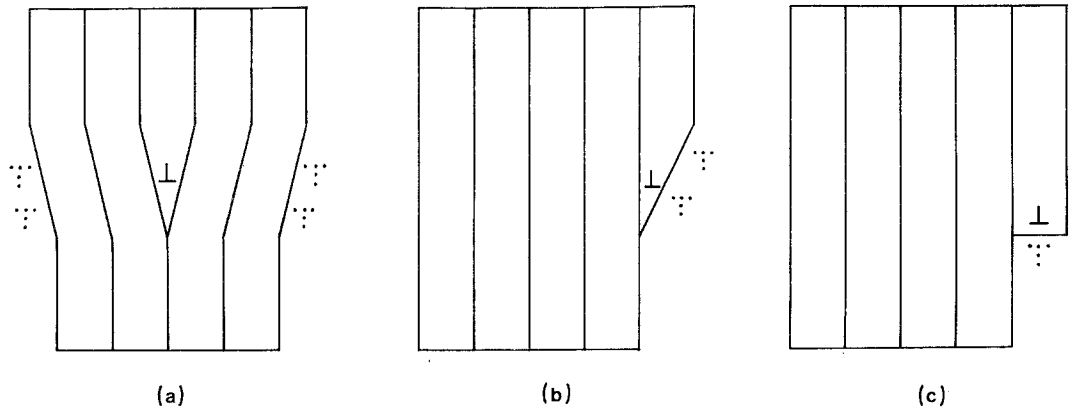

Figure 4 (a) Edge-type dislocation within a finite body. After dislocation in (a) has moved to surface and (b) not undergone or (c) undergone annihilation with surface dislocations.

configuration depicted in Fig. 3b would be the logical choice, since each cell would have rotated into a position where the maximum resolved shear stress on each of the two slip systems was essentially the same. The model shown in Fig. 3b is also appealing from the point of view that it allows very high densities of dislocations to exist within the cell walls without giving rise to corresponding large misorientations across the walls, in agreement with experimental observations. On the other hand, the configurations depicted in Figs. 3a and b correspond to limiting cases, and in reality, most cell walls will consist of combinations of both, i.e. possess tilt boundary and dipole character, depending upon local conditions within the crystal.

One of the more interesting aspects of the cell wall configurations of Figs. 3a and b is that they both posses low energies of about the same magnitude. This can be most easily seen by making use of surface dislocation considerations. In particular, consider the edge dislocation within a finite body, as depicted in Fig. 4. In order to satisfy the stress-free boundary conditions on the surface of the body originating from the stress field of the lattice dislocation, an array of surface dislocations (shown dotted) must be distributed over these surfaces [1, 2, 13]. It is in fact the surface dislocations which account for the distortions; i.e. shape change, associated with the outer surfaces of the finite body. As the lattice dislocation moves toward the surface, the surface dislocations are pulled closer to the lattice dislocation, as illustrated in Fig. 4b. It is important to note, however, that the lattice and surface dislocations in this figure are not yet combined. Combination in fact gives rise to the ledge configuration depicted in Fig. 4c, and corresponds to the reaction given by Equation 1 towards the right. It follows that all of the eleastic distortion is removed by the complete combination of surface and lattice dislocations.

If now an edge-type dislocation dipole within a finite body is considered, the configuration shown in Fig. 5 is obtained. In this particular case, all of the surface dislocations associated with the pair of lattice dislocations annihilate one another so that the outer surface of the finite body remains undistorted. This result also follows from St Venant's principle which states that at distances

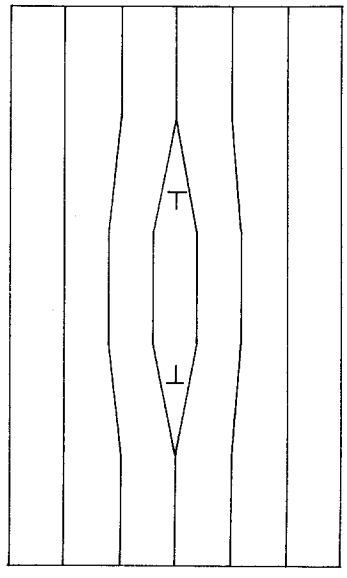

Figure 5 Dislocation dipole within a finite body.

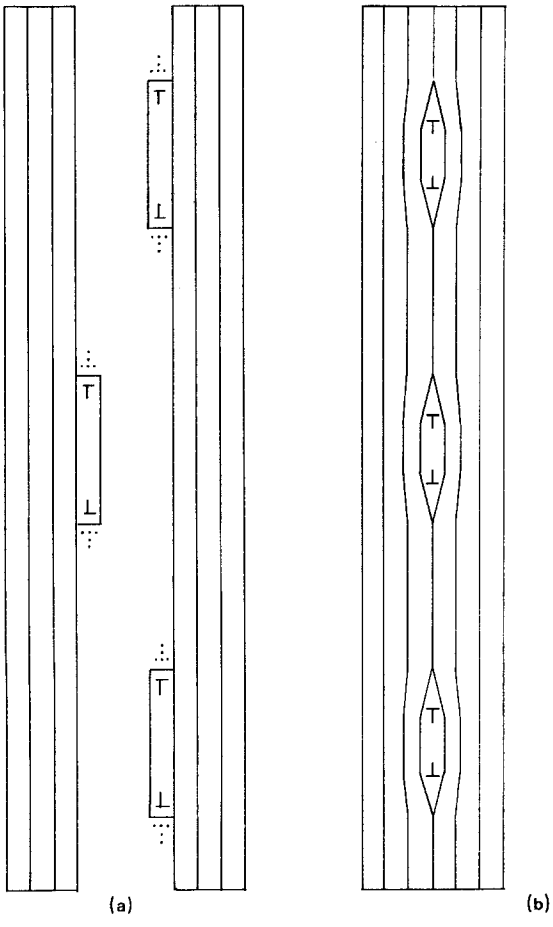

Figure 6 Joining of the two sets of surface ledges in (a) to form the vertical array of dislocation dipoles in (b).

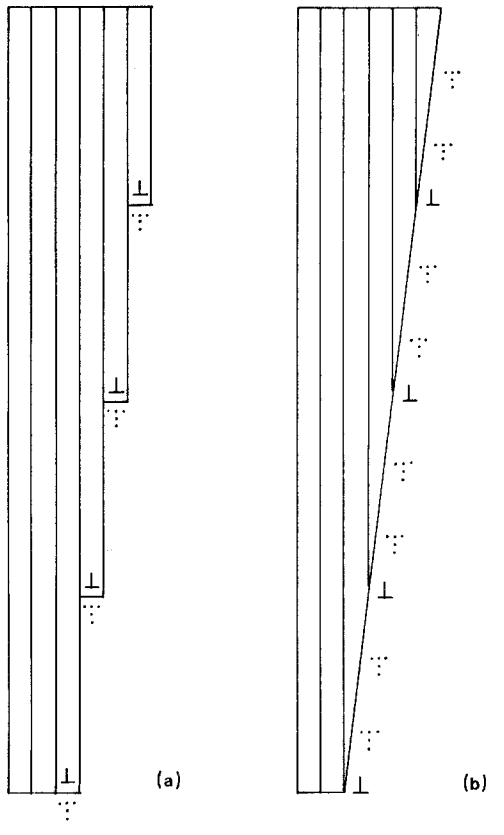

Figure 7 Flattening of the surface ledges in (a) to form the smooth surface shown in (b).

on the order of the separation between the various sources of stress, they can be considered as a combined entity [20].

A vertical array of dislocation dipoles can be formed by first considering the pair of half spaces depicted in Fig. 6a, each face of which contains ledges of the type shown in Fig. 4c, but which alternate in sign. If these two half spaces are forced into coalescence, the surface dislocations annihilate one another, while the lattice dislocations form a vertical array of edge-type dipoles, as illustrated in Fig. 6b. This particular array of dislocations is of relatively low energy since the distortions are limited to a distance of the order of the separation between the dipoles, and thus accounts for the stability of the cell wall configuration shown in Fig. 3b.

In order to comprehend fully the fundamental significance of the tilt-type boundary, let us first consider the half space shown in Fig. 7a whose surface contains equally-spaced ledges of the same sign. If now the ledges are eliminated by flattening the stepped surface, the configuration in Fig. 7b obtains. The elimination of the ledges by this process is equivalent to the reaction given by Equation 1 towards the left which in effect uncouples the surface dislocations from the lattice dislocation. The half space of Fig. 7b can next be combined with its mirror image to generate the symmetric tilt boundary of Fig. 8. A tilt boundary may thus be viewed as an alternating array of lattice and surface dislocations of opposite sign [21–23]. In this respect, it closely resembles the array of dislocation dipoles illustrated in Fig. 6b. The relatively low energy of the cell wall configuration in Fig. 3a is thus readily accounted for.

Suppose now that the plastic deformation depicted in Fig. 3b is confined to the upper surface of the body. The dislocation configuration illustrated in Fig. 9a would then obtain. Note that the cell wall morphology would be identical to that given in Fig. 3b, except for one important difference. In particular, the dislocation array at

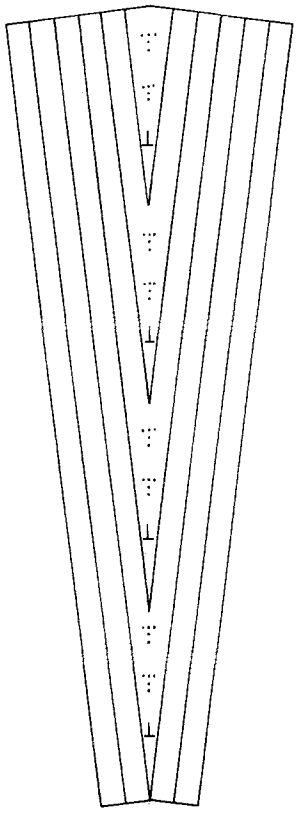

Figure 8 Tilt boundary of misorientation 14.25° formed by joining the inclined surface of Fig. 7b to its mirror image.

the junction between plastically deformed and undeformed regions now consists of a horizontal array of edge-type dislocations of the same sign whose Burgers vectors lie parallel to the junction. The effect of this array of dislocations is shown in Fig. 9b which is a somewhat more schematic version of Fig. 9a. In particular, the horizontal array of lattice dislocations gives rise to long-range stresses which induce surface dislocations on the faces of the body so as to insure stress-free boundary conditions. It is also clear that the plastic deformation associated with Fig. 9b has caused the lateral dimensions of the deformed layer to increase. If the plastic distortions in the upper half of the body shown in Fig. 9a were of the type shown in Fig. 3a rather than Fig. 3b, the configuration depicted in Fig. 9b would still obtain. The significance of this highly stressed interface between deformed and undeformed crystal with respect to wear will be the subject of further discussion.

Just as the lattice dislocations arranged themselves in the form of cell walls in Fig. 3 in response to a compressive stress, such is also expected to be the case if the externally applied stress is one of shear. This can be seen by reference to Fig. 10a where, as in the case of Fig. 3a, only a single slip system is allowed to be activated within each cell. However, unlike the case shown in Fig. 3a, the arrangement in Fig. 10a generates stresses which are of the order of the cell dimensions rather than the spacing between dislocations within the cell walls. This occurs because the dislocations within each segment of cell wall are all of the same sign with Burgers vectors parallel to the wall. This configuration is thus expected to be of somewhat higher energy than that depicted in Fig. 3a. However, if double slip is allowed to occur within each cell, the cell wall will consist of arrays of dislo-

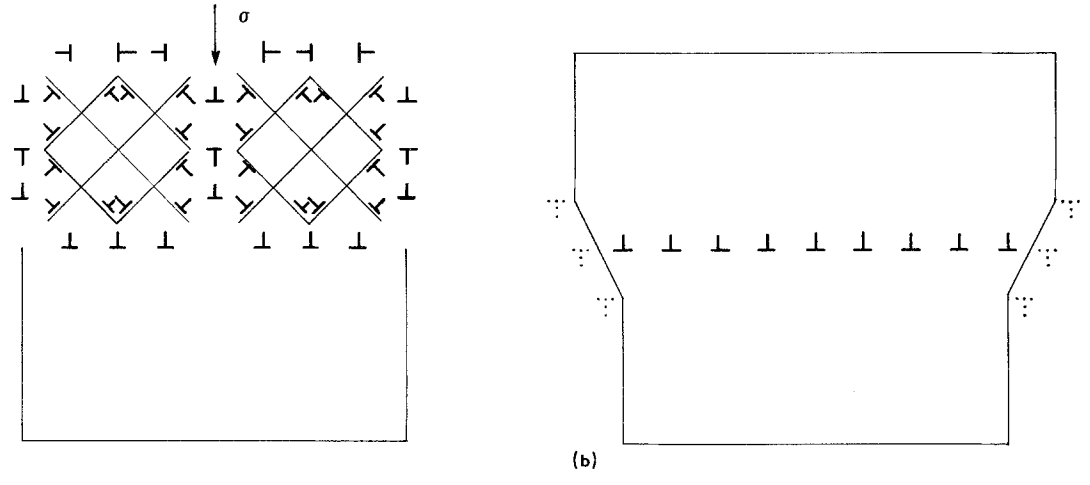

Figure 9 (a) Same as Fig. 3b, but with plastic deformation confined to the upper half of body. (b) Schematic illustration of the shape change associated with the deformation in (a).

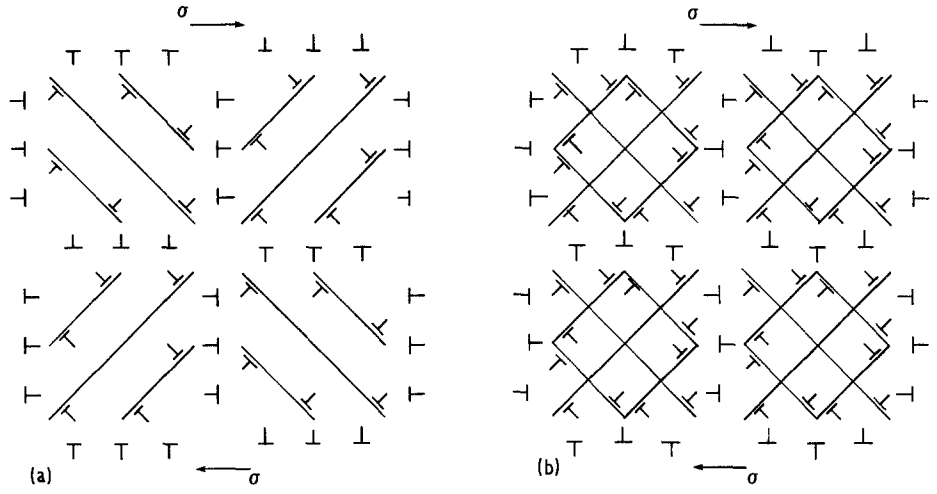

Figure 10 Cell wall formation in two dimensions under shear via (a) single and (b) double slip within each cell.

cation dipoles as illustrated in Fig. 10b. Unlike the case shown in Fig. 3b, the dipoles in Fig. 10b have their Burgers vectors parallel to the cell walls. This however has no significant effect on the energy, so that the energies of the configurations depicted in Figs. 3b and 10b are expected to posses very nearly the same relatively low value.

If, however, the plastic shear distortion of Fig. 10b is confined to the upper half of the crystal, the cell wall configuration illustrated in Fig. 11a obtains. In this particular instance, unlike the case associated with compressive distortions in Fig. 9a, the interface between the deformed and undeformed regions comprises a horizontal array of dislocations of like sign with Burgers vectors normal to the array, i.e. a symmetric tilt boundary. As we have already seen in connection with Fig. 8, any complete description of a tilt boundary must include the lattice dislocations along with the corresponding surface dislocations. A more schematic version of Fig. 11a is therefore redrawn in Fig. 11b to emphasize this important consideration. It thus follows that unlike the case depicted in Fig. 9b, the junction between deformed and undeformed crystal in Fig. 11b has associated with it only short-range stresses, and is thus of relatively low energy.

4. Mechanism of delamination

In order to understand how a cell wall could act as a preferred site for crack nucleation and growth, let us first consider the behaviour of a crack within

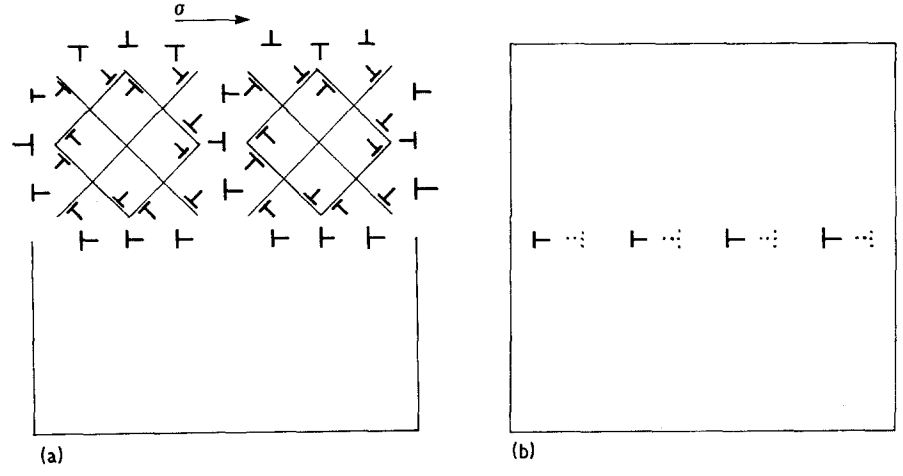

Figure 11 (a) Same as Fig. 10b, but with plastic deformation confined to the upper half of the body. (b) Simplified version of (a), showing surface dislocations.

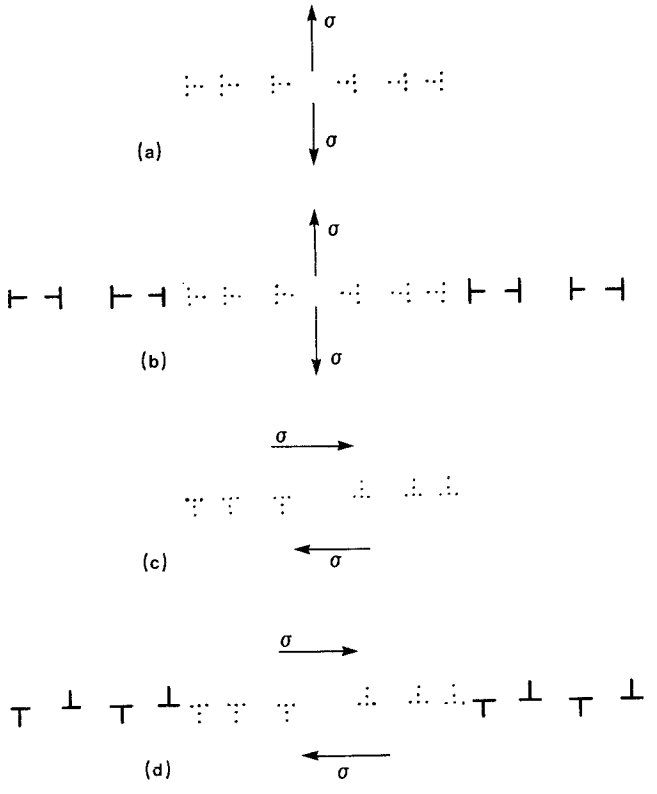

Figure 12 Tensile crack (a) within a perfect crystal, (b) along a cell wall. Shear crack (c) within a perfect crystal, (d) along a cell wall.

a perfect crystal. In particular, Fig. 12a depicts an elastic tensile type crack in terms of an array of surface dislocations [1, 2]. The total energy of such a crack can be written as:

$$E_T = E_S + E_I + E_\gamma - E_\sigma \qquad (2)$$

where E_S is the self energy of all the surface dislocations, E_I their total interaction energy, E_γ is the surface energy of the crack, while E_σ is the work done on the crack dislocations by the applied stress.

If now a tensile crack forms along a cell wall which consists of dislocation dipoles, such as illustrated in Figs. 3b, 11a or 11b, the configuration shown in Fig. 12b obtains. The dipoles are denoted by solid symbols. Each dipole has associated with it an energy per unit length of cell wall given by [24]

$$E_D = \frac{\mu b^2}{4\pi r(1-\nu)}\left[\ln\left(\frac{r'}{r_0}\right) + \frac{1}{2}\right] \qquad (3)$$

where μ is the shear modulus, b the Burgers vector of the dislocations comprising the dipole, ν is Poisson's ratio, r' the extension of the dipole, and r_0 the core radius of the dislocation. Since the dipoles are annihilated by crack formation, the energy given by Equation 3 is released and Equation 2 now becomes

$$E_T = E_S + E_I + E_\gamma - E_D - E_{\sigma'}. \qquad (4)$$

We may now define a new effective surface energy given by

$$E_{\gamma'} = E_\gamma - E_D. \qquad (5)$$

For r' in Equation 3 about $6b$, it is a simple matter to show that E_D becomes nearly the same as E_γ, so that crack formation and propagation becomes enormously simplified along cell walls for this reason alone. There is yet another contribution which reduces the energy for crack formation along the cell wall in Fig. 12b. This is due to the fact that the applied stress does work as the pair of dislocations comprising the dipoles move toward one another in response to this stress. This energy contribution per unit length of cell wall is given by

$$E_{D\sigma} = \frac{\sigma b r'}{2r'}. \qquad (6)$$

The total energy associated with the applied stress in Equation 4 is thus

$$E_{\sigma'} = E_\sigma + E_{D\sigma} \qquad (7)$$

where E_σ is the work done by the applied stress on

the crack dislocations alone. As in the case of E_D given by Equation 3, $E_{D\sigma}$ can also be quite large, i.e. of the order of the surface energy, E_γ.

The arguments given above for tensile cracks also apply to shear-type cracks. In particular, Fig. 12c depicts an elastic shear crack within a perfect crystal. When the elastic shear crack is allowed to form along a cell wall of the type shown in Fig. 10b, which again comprises dislocation dipoles, but of different orientation to those shown in Fig. 3b, the crack configuration illustrated in Fig. 12d obtains. The same arguments that were used for the tensile crack can also be extended to the shear-type crack. In particular, the energies associated with the shear cracks of Figs. 12c and d can be represented by Equations 2 and 4 respectively.

Tensile cracks of the type shown in Fig. 12b can be immediately ruled out in the case of sliding-type wear since the external stresses associated with this wear mechanism involve compressive as well as shear stresses. It is also clear from Fig. 9 that the compressive stresses *per se* do not contribute to crack nucleation and growth, but instead gives rise to the dislocation substructure which facilitates easy crack growth.

Although we have already seen that a shear crack can easily form at cell walls of the dipole type shown in Fig. 10b, the dislocation interface shown in Fig. 9b is of particular interest with respect to shear crack growth. The reason for this is that the dislocation configuration has associated with it long-range stresses, and thus correspondingly high strain energies. Upon application of an applied stress, σ, the strain energy can be relieved by the formation of an asymmetric shear crack, as shown in Fig. 13a. The creation of the crack involves the rearrangement of the uniformly spaced interface dislocations into a pile-up of crack dislocations with the same total Burgers vector. As a rough approximation, the dislocation configuration depicted in Fig. 9b can be simplified to that shown in Fig. 13b, while that illustrated in Fig. 13a can be redrawn as shown in Fig. 13c. The crack dislocation is now represented as a single dislocation. Furthermore, the crack is assumed to be small compared with the specimen dimensions and located near the centre of the body. This ensures that there is virtually no change in interaction energy between the crack dislocation with the misfit and surface dislocations for the relatively small change in position of the crack

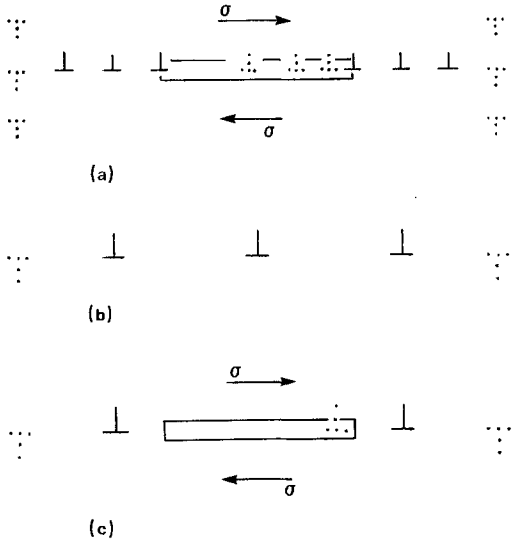

Figure 13 (a) Formation of an asymmetric shear crack at the dislocation interface shown in Fig. 9b. Simplification of (b) Fig. 9b, (c) Fig. 13a.

dislocation. Under these conditions, the energy associated with the crack may be written as

$$E_T = E_\gamma - E_\sigma. \tag{8}$$

Comparison of the above relation with Equation 2 shows that E_S and E_I are zero since no crack dislocations need be created, as they are already present as interface dislocations, and secondly, they are assumed to be combined into a single superdislocation. Equation 8 can be expanded to yield

$$E_T = \gamma r - \sigma b \frac{r}{2} \tag{9}$$

where γ is the energy per unit area associated with the crack surface, while r is the extension or length of the crack. It is clear from examination of Fig. 9b that the misfit dislocation density per unit length of interface is simply

$$\rho = \frac{w - w_0}{w_0} \tag{10}$$

where w and w_0 are the widths of the body before and after plastic deformation respectively. If the distortions are not too large, we can write

$$\frac{w - w_0}{w_0} = \frac{\Delta L}{L_0} = \epsilon \tag{11}$$

where L_0 is the thickness of the deformed layer, ΔL the decrease in thickness brought about by the deformation, while ϵ is the nominal strain. The

value for b in Equation 9 is thus simply

$$b = \epsilon r \tag{12}$$

so that Equation 9 becomes

$$E_T = \gamma r - \tfrac{1}{2}\sigma\epsilon r^2. \tag{13}$$

A maximum value of E_T occurs for the condition corresponding to $\partial E_T/\partial r = 0$ and yields

$$\sigma_c = \frac{\gamma}{\epsilon r_c}. \tag{14}$$

Thus, cracks with a size greater than r_c will grow spontaneously with a continuous decrease in energy. Equation 14 is somewhat analogous to the Griffith condition associated with the formation of an elastic crack in an otherwise perfect crystal, which is given by [2, 25]

$$\sigma_c = \left(\frac{2\gamma E}{\pi r_c}\right)^{1/2} \tag{15}$$

where E is Young's modulus. The value of σ_c given by Equation 14, however, is about one thousandth the value of that given by Griffith's equation. The main reason for this is that, unlike the case for the Griffith crack, no crack dislocations need be created to form the asymmetric shear crack at the plastic–elastic interface in Fig. 13c. Thus, shear crack formation and subsequent propagation with ultimate delamination of the plastically deformed surface layer, based upon the model depicted in Fig. 13c, is a relatively easy process. In addition, Equation 14 shows that the higher the amount of plastic strain, the lower the crack propagation stress, as expected on physical grounds.

In general, it is expected that sliding or adhesive wear will involve compressive as well as shear distortions. The highest internal stresses occasioned by these distortions are expected to be concentrated at the plastic–elastic interface. Although this interface may possess the tilt-type character of the type portrayed in Fig. 11b, as well as the misfit-type character, as shown in Fig. 9, it is the latter configuration that will respond to the shear component of the applied stress in the form of asymmetric shear-type cracks. It seems logical to assume that the wear rate $\dot{\omega}$ will be proportional to the number of pre-existing crack nuclei, N, i.e.

$$\dot{\omega} \alpha N. \tag{16}$$

The number of these nuclei would in turn be inversely proportional to their size, r_c, so that Equation 16 becomes

$$\dot{\omega} \alpha \frac{1}{r_c}. \tag{17}$$

In view of Equation 14, the above relation can be written as

$$\dot{\omega} \alpha \frac{\epsilon \sigma_c}{\gamma}. \tag{18}$$

Since σ_c is proportional to the force P acting normal to the wear surface via the coefficient of friction, Equation 18 becomes

$$\dot{\omega} \alpha \frac{\epsilon P}{\gamma}. \tag{19}$$

Assuming next that the amount of plastic strain ϵ is inversely proportional to the hardness, H, Equation 19 can be written as

$$\dot{\omega} = \frac{k}{\gamma}\frac{P}{H} \tag{20}$$

which is simply the well-known wear equation first developed by Archard [26, 27].

5. Summary and conclusions

The present study has shown that the concept of surface dislocations is a powerful one for the study of distortions within a body in general, and for local distortions near the surface of the body in particular. Since the phenomenon of wear is essentially one which involves surface distortions. The application of surface dislocations to this problem seems to be a natural choice. Preliminary theoretical studies contained in the present investigation show that sliding or adhesive wear can be readily accounted for in terms of delamination of the plastically deformed surface layer from the remaining undeformed body. The dislocation configuration at the interface between the deformed and undeformed regions is such as to make shear crack initiation and growth at this interface relatively easy. It is apparent from Equations 19 and 20 that perhaps the most important aspect of the wear problem concerns the amount of plastic deformation induced into the surface layers of the body under consideration. This degree of deformation will depend upon the work hardening characteristics. This degree of deformation will depend upon the work hardening characteristics, being low for materials that work harden rapidly, and high for low work hardening substances. Having taken this initial step, it seems to be a relatively simple matter to extend the surface

dislocation concept to include abrasive wear as well as impact or erosive wear.

Acknowledgement

The present research was supported by the United States Department of Energy under Contract No. DE-AS05-76ER0395.

References

1. M. J. MARCINKOWSKI, "Unified Theory of the Mechanical Behavior of Matter" (John Wiley & Sons, New York, 1979).
2. K. JAGANNADHAM and M. J. MARCINKOWSKI, "Unified Theory of Fracture" (Trans Tech. Publications, Aedermannsdorf, Switzerland, 1983).
3. N. P. SUH, *Wear* **25** (1973) 111.
4. *Idem, ibid.* **44** (1977) 1.
5. J. R. FLEMING and N. P. SUH, *ibid.* **44** (1977) 39.
6. A. R. ROSENFIELD, *ibid.* **61** (1980) 125.
7. Idem, ibid. 72, (1981) 97.
8. *Idem, ibid.* **72** (1981) 245.
9. I. I. GARBOR and J. V. SKORININ, *ibid.* **51** (1978) 327.
10. D. A. RIGNEY and W. A. GLAESER, *ibid.* **46** (1978) 241.
11. R. N. GARDNER and H. G. F. WILSDORF, *Met. Trans. A* **11** (1980) 659.
12. R. N. GARDNER, T. C. POLLOCK and H. G. F. WILSDORF, *Mater. Sci. Eng.* **29** (1977) 169.
13. K. JAGANNADHAM and M. J. MARCINKOWSKI, *Mater. Sci. Eng.* **38** (1979) 259.
14. J. D. EMBURY, A. S. KEH and R. M. FISHER, *Trans, Met. Soc. AIME* **236** (1966) 1252.
15. J. B. AUSTIN, *Trans Iron and Steel Inst. Jpn.* **19** (1979) 719.
16. J. J. JONAS, "Proceedings ICSMA 1", *Trans, Jpn. Inst. Metals* Supplement 9 (1968) 257.
17. H. MECKING, "Dislocation Modelling of Physical Systems", edited by M. F. Ashby, R. Bullough, C. S. Hartley and J. P. Hirth (Pergamon Press, New York, 1981) p. 197.
18. C. LANGFORD and M. COHEN, *Met. Trans.* **6A** 1975) 901.
19. D. KUHLMANN-WILSDORF and J. H. VAN DER MERWE, *Mat. Sci. Eng.* **55** (1982) 79.
20. Y. C. FUNG, "Foundations of Solid Mechanics" (Prentice-Hall, Englewood Cliffs, New Jersey, 1965).
21. M. J. MARCINKOWSKI, *Phys. Status Solidi (a)* **60** (1980) 109.
22. *Idem, J. Mater. Sci.* **18** (1983) 827.
23. *Idem, Phys. Status Solidi (a)* **73** (1982) 409.
24. A. H. COTTRELL. "Dislocations and Plastic Flow in Crystals" (Clarendon Press, London, 1953).
25. *Idem,* "The Mechanical Properties of Matter" (John Wiley and Sons, New York, 1964).
26. J. F. ARCHARD, *J. Appl. Phys.* **24** (1953) 981.
27. A. D. SARKAR, "Friction and Wear" (Academic Press, London, 1980).

Received 3 June
and accepted 28 July 1983